DOI: 10.1002/ppsc.201800359

**Article type: Full Paper**

# Structure Analysis of Solid Lipid Nanoparticles for Drug Delivery: A Combined USANS/SANS Study

*Rohan M. Shah*, Jitendra P. Mata, Gary Bryant, Liliana de Campo, Alexander Ife, Avinash V. Karpe, Snehal R. Jadhav, Daniel S. Eldridge, Enzo A. Palombo, Ian H. Harding*

Dr. R. M. Shah, Mr. A. Ife, Dr. D. S. Eldridge, Prof. E. A. Palombo, Prof. I. H. Harding

Department of Chemistry and Biotechnology, School of Science, Swinburne University of Technology, PO Box 218, Hawthorn, Melbourne, VIC 3122, Australia
E-mail: rshah@swin.edu.au

Dr. J. P. Mata, Dr. L. de Campo

Australian Centre for Neutron Scattering, Australian Nuclear Science and Technology Organization (ANSTO), Sydney, NSW 2234, Australia

Prof. G. Bryant

Centre for Molecular and Nanoscale Physics (NanoPHYS), School of Science, RMIT University, Melbourne, VIC 3001, Australia

Dr. A. K. Karpe

Land and Water, Commonwealth Scientific and Industrial Research Organization (CSIRO), Brisbane, QLD 4001, Australia

Dr. S. R. Jadhav

Centre for Advanced Sensory Science, School of Exercise and Nutrition Sciences, Deakin University, Melbourne, VIC 3125, Australia

**Keywords:** small angle neutron scattering (SANS), ultra-small angle neutron scattering (USANS), solid lipid nanoparticles, Guinier-Porod model, ellipsoidal model

Suspensions of solid lipid nanoparticles (SLNs) stabilized with emulsifiers have been extensively investigated as drug carriers since the 1990s, although details of their ultrastructure are poorly defined. Previously, our group reported a novel microwave- assisted microemulsion-based technique to prepare SLNs. To understand the detailed internal structure of these SLNs, ultra-small angle neutron scattering (USANS) and small angle neutron scattering (SANS) experiments were conducted on suspensions of hydrogenated stearic acid SLNs stabilized with hydrogenated Tween 20 surfactant in $D_2O$. Together, SANS and USANS gave a combined Q range of 0.000047 to 0.6 $Å^{-1}$ (corresponding to a size range of ~1nm-15μm). This extended Q range allows a comprehensive understanding of the hierarchical structure of SLNs. The data are consistent with the multi-length scale structure of SLNs having polydispersed large particles with roughened surfaces at the microscale level. At the nanoscale level, the results are consistent with the SLNs solution having an ellipsoidal shape intermediate between spheres and rods, with a crossover from mass fractals to surface fractals. The elucidation of this structure is particularly important given that the structure influences the stability and drug release properties of the nanoparticles. These results will assist in the development of systems with desired shape and properties.

## 1. Introduction

Nano carriers have been explored for delivery of therapeutics for over 35 years. Several products have been approved worldwide since the introduction of the first liposomal system, Doxyl®. Nano carriers have been applied to (1) delivery of drugs and other bioactives, (2) in vitro diagnostics to enhance biomarker sensitivity, (3) functionalization of biomaterial surfaces to enhance the performance of implants and (4) in vivo imaging.[1] Various advanced nanostructures have been

developed for this purpose including micelles, liposomes, polymeric nanoparticles and lipid nanoparticles.

Solid lipid nanoparticles (SLNs) have been extensively investigated since their inception in the 1990s.[2, 3] SLNs are made from emulsions at high temperature that crystallize predominantly into SLNs upon cooling. The encapsulation of drugs within the solid lipidic matrix serves two important functions: (1) to protect the drugs from chemical degradation; and (2) to modulate the drug release profile. Suspensions of SLNs have many of the desirable features of other nanostructures (biocompatibility, increased drug payload, controlled release, physical stability) but with reduced negative effects associated with those nanostructures (drug leakage, polymer and solvent toxicity).[4] Cell culture studies have shown that the SLNs are non-toxic and easily taken up by human epithelial cells.[5]

Our group has recently reported a novel microwave-assisted technique for producing SLNs yielding colloidal particles from a microemulsion template.[6] Our previous experiments indicate the suitability of these SLNs as potential drug carriers. A variety of characterization experiments (particle size analysis, zeta potential measurements, drug loading and encapsulation efficiency studies, thermal analysis, X-ray diffraction studies) definitively showed that the microwave-based procedure produces SLNs with small size, moderate zeta potential, high encapsulation efficiency and reduced crystallinity. A wide range of drugs with different physicochemical properties has been successfully encapsulated into these carrier systems.[6-9]

SLNs loaded with drugs from different categories show diverse drug release patterns.[10] This may be due to the different classes of drug collecting in different locations on, or within, the SLNs. Despite

these differences, drug release studies generally suggest core-shell structures for SLNs with drug-enriched cores or drug-enriched shell structures resulting in different sizes and shapes.[10-12] So far, very little has been reported about the physical characteristics of SLNs, such as nano- and micro-structure, that influence the release behaviour of encapsulated drugs and their subsequent stability. For a better understanding of SLNs and their development as drug vehicles, it is necessary to study the ultrastructure of this lipid matrix. Ultrastructure generally relates to interior of the particle and can relate to internal partitioning through, for example, a core-shell structure. It can also relate to the formulation itself, including the particle itself, but can also include structures such as micelles, which may be simultaneously present.[13]

Small angle neutron scattering (SANS) has been widely used to study the several nanomaterials including micelles, polymeric nanoparticles and liposomes in solution. Recently, Gómez-Graña et al. demonstrated the use of small angle scattering techniques to determine the thickness of surfactant layers on gold nanorods.[14] Filippov et al. performed time-dependent small angle scattering measurements at several pH conditions to characterize the drug release and changes in size and shape of polymer micelles.[15] Balgavý et al. investigated the bilayer thickness and lipid interface area in unilamellar extruded 1,2-diacylphosphatidylcholine liposomes using SANS.[16] Although several reports have been published on the use of SANS in nanoparticle research, the literature on structure analysis of SLNs using neutron scattering is very limited and this area of research remains largely unexplored.

In the current work, detailed studies were undertaken to characterize the SLN structure using a combination of ultra-small angle neutron (USANS) and small angle neutron scattering (SANS) covering a wide range of scattering vector Q. The SANS data in the Q range $\geq 1 \times 10^{-2}$ $Å^{-1}$ provides

information on the ultrastructure of SLNs at nanoscale, while combined SANS and USANS data in the Q range ≤ 1 × $10^{-2}$ $Å^{-1}$ provide information about the particle size, shape/structure and interparticle interaction at microscale.[17] The extended Q range used in this study allowed us to undertake an extensive study of the hierarchical structure of SLNs. To the best of our knowledge, this is the first detailed study of SLN structure using neutron scattering techniques.

**2. Results and Discussion**

To ensure a good fit of the data when combined, a sufficient overlap of the USANS and SANS data is required, allowing a combined plot of absolute intensity ($cm^{-1}$) vs. Q ($Å^{-1}$). The combined data from USANS and the three SANS configurations, demonstrating the consistency of the techniques are shown in **Figure S1** (see **Supplementary Information)**. This broad Q range provides information on the structure of SLNs on multiple length scales. The merged data shows two shoulders, and for easier interpretation, are split into two regimes of different Q ranges. Roughly, the low-Q to mid-Q region (i.e. first shoulder region in **Figure S1**, i.e. Q ≤ 1 × $10^{-2}$ Å) gives information on the micron scale. This covers the particle size of the SLNs. The mid-Q to high-Q region (i.e. second shoulder region in **Figure S1**, i.e. Q ≥ 1 × $10^{-2}$ Å) gives information on the nanoscale. This covers the ultrastructure in the SLN particles.

SAS data are commonly analyzed using standard linear plots such as Guinier or Porod plots. The Guinier approximation [26] is easily performed to give an estimation of 'particle size' i.e. radius of gyration at macroscale (denoted by $R_g$, see **Equation (1)**).

$$I(Q) = G \exp\left(\frac{-Q^2 R_g^2}{3}\right)$$

… **Equation (1)**

where G is the scale factor.

The Porod model gives an approximate physical form i.e. internal structure of the scattering entity from the Porod exponent at the nanoscale. **Equation (2)** represents the relationship that defines this model.

$$I(Q) = \frac{C}{Q^d} + \text{incoherent background}$$

… **Equation (2)**

where C is the scale factor and d is the Porod exponent.

**Table 1** summarizes the various Porod exponents and the corresponding physical forms of the scattering entity.

A possible mass fractal interpretation (such as branched systems or networks) is indicated by $d < 3$ and for surface fractals, $3 \leq d \leq 4$.[27]

The Guinier and the Porod models are typically applied across a limited scattering vector range. Hammouda combined these two models and introduced a generalized Guinier-Porod empirical model.[27] This model has applicability over a wide range of scattering vectors and can be used to derive information about the physical properties of the scattering particle. Hammouda's generalized

Guinier-Porod empirical model has found to be applicable by many researchers.[28-31] The scattering intensity I(Q) for Hammouda's generalized Guinier-Porod empirical model is given by **Equation (3)**. The Guinier form (see **Equation (1)**) is used for $Q \leq Q_1$ and the Porod form (see **Equation (2)**) is used for $Q \geq Q_1$. This function includes the crossover from Guinier to Porod fitting at the scattering variable $Q_1$.

$$I(Q) = \begin{cases} \frac{G}{Q^s} \exp\left(\frac{-Q^2 R_g^2}{3-s}\right) \ldots \text{for } Q \leq Q_1 \\ \frac{A}{Q^d} \ldots \text{for } Q \geq Q_1 \end{cases}$$

… **Equation (3)**

These equations are useful to estimate $R_g$. In this equation, s is the dimensional variable and helps model both spherical and non-spherical objects. For scattering due to 3-D globular objects such as spheres, s = 0. For structures such as rods, s = 1 and for 1-dimensional objects such as lamellae or platelets or discs, s = 2. The dimensionality parameter $D_p$ is defined as $D_p = 3 - s$. The denominator (3 – s) in **Equation (3)**, therefore, becomes 3 for spherical objects, 2 for rods and 1 for plates. Assuming there is continuity at the crossover $Q_1$, the following relationships are obtained (see **Equation (4) and (5)**),

$$Q_1 = \frac{1}{R_g}\left(\frac{(d-s)(3-s)}{2}\right)^{1/2}$$

… **Equation (4)**

$$D = G \exp\left(\frac{-Q_1^2 R_g^2}{3-s}\right) Q_1^{(d-s)} = G \exp\left(\frac{-(d-s)}{2}\right)\left(\frac{(d-s)(3-s)}{2}\right)^{(d-s)/2} \frac{1}{R_g^{(d-s)}}$$

… **Equation (5)**

The slope at low Q provides information on particle conformation; plateaus indicating spherical particles with an increasing slope indicating an elongated shape.[30] The slope in the low-Q region of the scattering intensity indicates qualitatively that they are elongated in solution. Non-linear least squares fits to the generalized Guinier-Porod model were performed in the two different Q ranges (i) $4.7 \times 10^{-5} – 1.1 \times 10^{-2}$ Å$^{-1}$ (referred to hereafter as the 'first Guinier-Porod region') and (ii) $1 \times 10^{-2} – 6 \times 10^{-1}$ Å$^{-1}$ (referred to hereafter as the 'second Guinier-Porod region'). It is worth noting that the Guinier-Porod model applied here is an empirical model applicable to objects of arbitrary shape and provides an estimate of the radius of gyration, $R_g$ and the dimensional variable, s. The merged data and the generalized Guinier-Porod model fits are shown in **Figure 1(a)**. The parameters for the generalized Guinier-Porod fits are summarized in **Table 2**.

The first Guinier-Porod region gives an excellent fit and provides information about the SLN sample at the microscale level (particle size characteristics). Over the reduced region $6 \times 10^{-4}$ Å$^{-1}$ < Q < $1 \times 10^{-2}$ Å$^{-1}$, the behaviour is a power law with slope of 2.5. This value was fixed for the Guinier-Porod fits over the larger Q range, to reduce the number of fit parameters. Similarly, d was fixed at 4.0 for the second Guinier-Porod region. A Porod exponent d < 3 indicates a possible mass fractal scattering from a scattering entity with a very rough surface.[27] The dimensionality parameter $D_p$ = 1.67, indicates a possible oblate structure intermediate between rods and lamellae or a sphere with high polydispersity. In one of the previous study, particles were characterised using multi-angle SLS/DLS and the results indicated particles with high polydispersity of 60%.[10] Using the values from **Table 2** and **Equation (4)**, the value of $Q_1$ becomes $9.871 \times 10^{-4}$ Å$^{-1}$ (marked as $Q_{G\text{-}P1}$) in **Figure 1(a)**.

We know from previous studies that scattering in the USANS region comes from the SLN suspension.[10] The hydrodynamic radius of the SLNs, measured by dynamic light scattering (DLS), was approximately 1360 Å.[10] In this study, the radius of gyration $R_g$ was found to be ~1001.3 Å (see **Table 2**). If the particles are spherical, this corresponds to a radius of ~1293 Å. The s value of 1.33 suggests an oblate structure or sphere with high polydispersity. As such structures have two length parameters, there is no easy way to relate the $R_g$ to a physical dimension without further information. This is also true of the hydrodynamic radius, which has contributions from both length and radius. So further analysis is not possible, however we can comment on the fact that the hydrodynamic radius (1360 Å) is slightly larger than the radius assuming a sphere. This is due to the following reasons that are well known within scattering community:

- the SLNs are stabilized with a layer of solvated Tween® 20 micelles, which has a hydrodynamic radius of 27 Å.[32] As the layer is solvated it will not contribute to the SANS scattering, but it will contribute to the hydrodynamic radius, making it larger by ~30 Å;
- particles moving under Brownian motion may carry a layer of solvent with them, further increasing the hydrodynamic radius; and
- if the particles are rough, the SANS radius represents the radius where there is a significant change in scattering length density (SLD), which will be closer to the inner radius of the "roughness". DLS measures the hydrodynamic radius, which will be closer to the maximum particle size (the outer radius of the "roughness", plus the solvation layer.

Thus, DLS will always give a slightly larger radius than techniques that rely on Q-dependent scattering (e.g. SANS or Static Light Scattering).[33, 34]

The second Guinier-Porod region provides information about the smaller scale structure of the sample, including the internal structure of the SLN particles, as well as the structure of possibly co-existing Tween 20 micelles. The radius of gyration $R_g$ of the scattering entity was found to be 20.3 Å. The value of $Q_2$ was determined to be $9.02 \times 10^{-2}$ $Å^{-1}$ using the fitting parameter values from **Table 2** in **Equation (4)**. This value is marked as $Q_{G\text{-}P2}$ in **Figure 1(a)**.

To confirm the approach used in fitting the generalized model, the experimental data over the entire Q range were fitted using a custom plugin model created in SasView. **Figure 1(b)** illustrates the customized model fir to the merged data. The plugin model function, which comprises of the sum of two Guinier-Porod functions, is shown in **Equation (6)**.

$$I(Q) = I(Q_1) + I(Q_2)$$

… **Equation (6)**

where $I(Q_1)$ and $I(Q_2)$ are the intensity scattering functions from first and second Guinier-Porod regions respectively.

The influence of both Guinier-Porod regions was studied using the sum function. The major correlation occurs between the d value of the first Guinier-Porod region and the s value and $R_g$ of the second Guinier-Porod region. The fitting was, thus, performed keeping all parameters fixed at the values determined earlier (see **Table 2**) while allowing d value of the first Guinier-Porod region and s value and $R_g$ of the second Guinier-Porod region to vary. It was found that $R_g$ decreased slightly from 20.2 (± 0.1) Å to 19.6 (± 0.1) Å and s value decreased slightly from 0.84 to 0.82, though the fit in the middle region is not as good fitting the two regions independently ($\chi^2 = 14.06$).

The dimensionality parameter $D_p$ of the scattering particles was found to be 2.16, which implies that the scattering particle has an intermediate ellipsoidal structure between spheres and rods,[27] which is consistent with surfactant micelles.[35] This was further supported by fitting the data in mid-Q to high-Q region ($5.6 \times 10^{-3}$ Å $\leq Q \leq 7.3 \times 10^{-1}$ Å) to an ellipsoidal model.[36] **Equation 7** gives the scattering intensity function for randomly oriented ellipsoids,

$$I(Q) = \int_0^1 \emptyset^2 \left[ Q.R_b\left(1 + x^2 (v^2 - 1)\right)^{\frac{1}{2}} \right] dx$$

… **Equation 7**

where

$$v = \frac{R_a}{R_b}$$

… **Equation 8**

$$F(Q,\alpha) = 3.\Delta\rho.V\frac{\sin(QR) - QR.\cos(QR)}{(QR)^3}$$

… **Equation 9**

For

$$R = [R_e^2 \sin^2\alpha + R_p^2 \cos^2\alpha]^{1/2}$$

… **Equation 10**

where α is the angle between the axis of the ellipsoid and $\underset{Q}{\rightarrow}$ and V is the volume of the ellipsoid given by,

$$V = \frac{4}{3}\pi R_p R_e^2 \quad \text{... Equation 11}$$

where $R_p$ is polar radius along the rotational axis of the ellipsoid, $R_e$ is the equatorial radius perpendicular to the rotational axis of the ellipsoid and Δρ is the difference in the scattering length densities of the scatterer and the solvent.

Tween 20 is a low molecular weight non-ionic surfactant with a very low critical micelle concentration (CMC) of 0.06 mM. The concentration of Tween 20 used in the formulation of SLNs is approximately 0.003 M, which is 50 times that of its CMC. **Figure 2** shows the scattering intensity from stearic acid and Tween 20 at volume fractions equivalent to that used in the SLN preparation. The SANS data for a 0.003 M Tween 20 solution in $D_2O$ fitted well ($\chi^2$ = 1.46) to the ellipsoidal shape of Tween 20 micelles is shown in **Figure 2**.

The scattering length densities of the sample and the solvent were fixed at $5.94 \times 10^{-5}$ Å$^{-2}$ and $6.39 \times 10^{-6}$ Å$^{-2}$ respectively. The value of the semi-minor axis and semi-major axes were 19.2 ± 0.1 Å and 38.4 ± 0.1 Å respectively and the scale factor was estimated to be 0.002. Mahajan et al. [35] suggested similar values for Tween 20 micelles in their study. The radius of gyration $R_g$ of tween 20 micelles was calculated the using **Equation 12**,

$$R_g = \sqrt{\frac{R_p^2 + R_e^2 + R_e^2}{5}}$$

… **Equation 12**

The $R_g$ of Tween 20 micelles was found to 21.1 Å. This value aligns well with the $R_g$ = 20.4 Å obtained from the Guinier-Porod model fitting (see **Table 2**).

In our previous study, the SAXS investigation of stearic acid-based SLNs showed a sharp peak at Q = 0.153 $Å^{-1}$.[10] Similar results were obtained by de Souza et al. [37] and Maruyama et al. [38], who demonstrated by SAXS that stearic acid is arranged in a lamellar lattice structure. Stearic acid crystals suspended in $D_2O$ also showed similar results by SANS **(Figure 2)**. We see no evidence of such a structure in the SANS data for SLNs. A likely explanation for this is that the internal structure of the particles consists of mostly lamellar crystalline sheets of stearic acid, with almost no $D_2O$ between the sheets, so there would be very low scattering contrast inside the particles, leading to no discernible peak.

The Tween 20 molecules, on the other hand, would be mostly excluded from these lamellar structures: a small fraction would stabilize the surface of the lamellar particles, with the vast majority forming separate micelles, due to their inherent hydrophilicity. Thus, it is likely that most of the scattering in the high-Q region comes predominantly from the Tween micelles. Excess of Tween 20 used in the formulation form separate micelles and most likely contribute to most of the scattering intensity in the high Q region. The volume fraction of Tween 20 in the SLNs is much higher than the volume fraction of stearic acid and this could explain the absence of a sharp peak corresponding to the lamellar structure of stearic acid in the SANS data for SLNs.

These findings give an estimation of the hierarchical structure of the SLNs. At the microscale, the findings suggest that the SLNs are oblate ellipsoidal in shape. These findings are based on the

assumption that the particles are monodispersed ellipsoids or spheres with high polydispersity. Our earlier findings have also suggested spherical structures with high polydispersity of 60%.[10] At the nanoscale, stearic acid could be forming lamellar structures and surface-stabilized with Tween 20 micelles. A customized model comprising of the Guinier-Porod and ellipsoidal models was used to fit the entire USANS/SANS ($\chi^2$ = 41.99) as shown in **Figure 1(c)**. All parameters were fixed at values determined earlier while allowing $R_g$ (for Guinier-Porod model at low Q) and scale factor (for ellipsoidal model at high Q) to vary. This custom model is shown in **Equation 13**,

$$I(Q) = I(Q_1) + I(Q_2)$$

**… Equation 13**

where $I(Q_1)$ and $I(Q_2)$ are the intensity scattering functions from the Guinier-Porod and ellipsoidal models respectively.

It was found that $R_g$ (at low Q) increased marginally from 1001.3 (± 45.3) Å to 1046.6 (± 2.6) Å. The mid Q slope could have some of underlying lamellar structure. The effect of underlying lamellar structure can be studied using deuterated stearic acid and/or deuterated Tween 20 solution and will be the subject of future research. At high Q, the scale factor (representing the volume fraction of Tween 20 micelles in the solution) reduced from 0.002 to 0.0012 when the SLNs were prepared. This further supports our understanding of the behavior of Tween 20 micelles in the formulation that a small fraction stabilizes the surface of the particles and the remaining forms separate micelles. Further shape-dependent analysis will be useful to ascertain the structure of SLNs. The structure may well differ when a drug is encapsulated within and/or on the surface of SLNs. This will be the subject of future research.

## 3. Conclusion

The results of this study provide important insights into the structure of SLNs, suggesting that the particles could have an intermediate oblate structure or spherical structure with high polydispersity and a rough surface at the microscale level. At the nanoscale level, the results suggest that particles are possibly made of intermediate ellipsoidal structures between spheres and rods of co-existing Tween 20 micelles and possibly lamellar stearic acid structures. The lamellar structure is being obscured by the scattering from excess Tween 20 micelles and therefore is not visible. A contrast variation SANS study using deuterated stearic acid and/or Tween 20 in the future will further our understanding of the structure of SLNs and aid in engineering of particles to impart controlled release properties to SLNs.

## 4. Experimental Section

*Preparation of solid lipid nanoparticles (SLNs)*: The method of preparation of SLNs has been described previously.[10] Briefly, accurately weighed quantities of stearic acid (0.10 g, Sigma-Aldrich, Australia), Tween® 20 surfactant (0.15 mL, Merck, Germany) and $D_2O$-water (1.35 mL, Sigma-Aldrich, Australia) were heated for 10 min at 80°C, with variable microwave power (not exceeding 18 W) and constant stirring, using a 2.45 GHz Discover LabMate microwave synthesizer (CEM Corp., USA). This constitutes a single-pot synthesis of an o/w microemulsion. The o/w microemulsion, while still hot, was dispersed in cold $D_2O$ (50 mL, ~ 6 - 8°C) under constant magnetic stirring for 30 min, resulting in precipitation of SLNs.

*Small angle neutron scattering (SANS) measurements*: The SANS measurements were performed on the 40 m QUOKKA instrument at the OPAL reactor.[18, 19] Three configurations were used to cover a Q range of $7 \times 10^{-4} - 6 \times 10^{-1}$ Å$^{-1}$. Q is the magnitude of the scattering vector and is defined by **Equation (14)**,

$$Q = \frac{4\pi}{\lambda} \sin\frac{\theta}{2} \quad \text{… Equation (14)}$$

where λ is the wavelength (Å) and θ is the scattering angle.

The configurations used were:

(i) Source-to-sample distance (SSD) and sample-to-detector distance (SDD) = 20.0 m with focusing lens optics using λ = 8.1 Å (Δλ/ λ = 10%);

(ii) SSD and SDD = 12.0 m, with λ = 5.0 Å (Δλ/ λ = 10%) and

(iii) SSD = 12.0 m and SDD = 1.3 m, with λ = 5.0 Å (Δλ/ λ = 10%)

The source and sample aperture diameters were 50.0 mm and 10.0 mm, respectively, for all configurations except for configuration (i) where the source aperture diameter was 10.0 mm. The SLNs were measured in quartz Hellma cells.

*Ultra-small angle neutron scattering (USANS) measurements*: The USANS measurements were performed using the KOOKABURRA instrument at the OPAL reactor.[20] The experiments were performed on samples identical to the ones used for SANS measurements. Using a neutron

wavelength of 4.74 Å and a Gd aperture with a diameter of 29 mm, a Q range of $4.7 \times 10^{-5} – 7 \times 10^{-3}$ $Å^{-1}$ was accessed.

*Data Reduction and Analysis*: SANS data were reduced using NCNR SANS reduction macros in the Igor software package (version 6.3.7.2, Wavemetrics, Lake Oswego, OR) originally written by Kline [21] and modified to accept HDF5 data files from the QUOKKA instrument.[22] The data were corrected for empty cell scattering, transmission, and detector response, and transformed onto an absolute scale by the use of an attenuated direct beam transmission measurement.[21] The USANS data were reduced with an empty Kookaburra cell data as background using Python scripts running in Gumtree based on the standard procedure[23] and converted to an absolute scale. The reduced slit-smeared data were de-smeared using Lake's iterative technique,[24] as implemented in the NIST data reduction macros[25] and subsequently merged with the SANS data. De-smearing the USANS data makes it easier to compare with the SANS data. Merged USANS/SANS data over the entire Q range were characterized using model-independent and model-dependent analysis using the SASView software package (version 4.1.2, http://www.sasview.org/).

**Supporting Information**

Supporting Information is available from the Wiley Online Library or from the author.

**Acknowledgements**

This work is supported by the ANSTO award P5527. This work also benefited from the use of the SasView application, originally developed under NSF award DMR-0520547. SasView also contains code developed with funding from the EU Horizon 2020 programme under the SINE2020 project Grant No 654000.

Received: ((will be filled in by the editorial staff))

Revised: ((will be filled in by the editorial staff))

Published online: ((will be filled in by the editorial staff))

[1] J. V. Natarajan, C. Nugraha, X. W. Ng and S. Venkatraman, *Journal of Controlled Release*, 2014, **193**, 122-138.

[2] M. Gasco, U. Patent, US5250236, 1993.

[3] R. Muller, C. Schwarz, W. Mehnert and J. Lucks, 1993.

[4] R. Shah, D. Eldridge, E. Palombo and I. Harding, in *Lipid Nanoparticles: Production, Characterization and Stability*, Springer International Publishing, Cham, 2015, DOI: 10.1007/978-3-319-10711-0_1, pp. 1-9.

[5] R. M. Shah, D. Rajasekaran, M. Ludford-Menting, D. S. Eldridge, E. A. Palombo and I. H. Harding, *Colloid Surface B*, 2016, **140**, 204-212.

[6] R. Shah, F. Malherbe, D. Eldridge, E. Palombo and I. Harding, *Journal of Colloid and Interface Science*, 2014, **428**, 286-294.

[7] R. M. Shah, D. S. Eldridge, E. A. Palombo and I. H. Harding, *Applied Materials Today*, 2016, **5**, 118-127.

[8] R. M. Shah, D. S. Eldridge, E. A. Palombo and I. H. Harding, *International Journal of Pharmaceutics*, 2016, **515**.

[9] R. M. Shah, D. S. Eldridge, E. A. Palombo and I. H. Harding, *European Journal of Pharmaceutics and Biopharmaceutics*, 2017, **117**, 141-150.

[10] R. M. Shah, G. Bryant, M. Taylor, D. S. Eldridge, E. A. Palombo and I. H. Harding, *RSC Advances*, 2016, **6**, 36803-36810.

[11] S. Bose, Y. Du, P. Takhistov and B. Michniak-Kohn, *International journal of pharmaceutics*, 2013, **441**, 56-66.

[12] V. K. Venishetty, R. Chede, R. Komuravelli, L. Adepu, R. Sistla and P. V. Diwan, *Colloids and Surfaces B: Biointerfaces*, 2012, **95**, 1-9.

[13] R. Shah, D. Eldridge, E. Palombo and I. Harding, in *Lipid Nanoparticles: Production, Characterization and Stability*, Springer, London, UK, 2015, ch. 4, pp. 45-74.

[14] S. Gómez-Graña, F. Hubert, F. Testard, A. Guerrero-Martínez, I. Grillo, L. M. Liz-Marzán and O. Spalla, *Langmuir*, 2012, **28**, 1453-1459.

[15] S. K. Filippov, J. M. Franklin, P. V. Konarev, P. Chytil, T. Etrych, A. Bogomolova, M. Dyakonova, C. M. Papadakis, A. Radulescu and K. Ulbrich, *Biomacromolecules*, 2013, **14**, 4061-4070.

[16] P. Balgavý, M. Dubničková, N. Kučerka, M. A. Kiselev, S. P. Yaradaikin and D. Uhríková, *Biochimica et Biophysica Acta (BBA)-Biomembranes*, 2001, **1512**, 40-52.

[17] M. Taghavikish, S. Subianto, N. K. Dutta, L. de Campo, J. P. Mata, C. Rehm and N. R. Choudhury, *ACS Omega*, 2016, **1**, 29-40.

[18] K. Wood, J. P. Mata, C. J. Garvey, C.-M. Wu, W. A. Hamilton, P. Abbeywick, D. Bartlett, F. Bartsch, P. Baxter, N. Booth, W. Brown, J. Christoforidis, D. Clowes, T. d'Adam, F. Darmann, M. Deura, S. Harrison, N. Hauser, G. Horton, D. Federici, F. Franceschini, P. Hanson, E. Imamovic, P. Imperia, M. Jones, S. Kennedy, S. Kim, T. Lam, W. T. Lee, M. Lesha, D. Mannicke, T. Noakes, S. R. Olsen, J. C. Osborn, D. Penny, M. Perry, S. A. Pullen, R. A. Robinson, J. C. Schulz, N. Xiong and E. P. Gilbert, *Journal of Applied Crystallography*, 2018, **51**, 294-314.

[19] E. P. Gilbert, J. C. Schulz and T. J. Noakes, *Physica B: Condensed Matter*, 2006, **385**, 1180-1182.

[20] C. Rehm, A. Brûlé, A. K. Freund and S. J. Kennedy, *Journal of Applied Crystallography*, 2013, **46**, 1699-1704.

[21] S. R. Kline, *Journal of applied crystallography*, 2006, **39**, 895-900.

[22] K. Aramaki, C. Iwata, J. Mata, T. Maehara, D. Aburano, Y. Sakanishi and K. Kitao, *Physical Chemistry Chemical Physics*, 2017, **19**, 23802-23808.

[23] T. Lam, N. Hauser, A. Götz, P. Hathaway, F. Franceschini, H. Rayner and L. Zhang, *Physica B: Condensed Matter*, 2006, **385-386**, 1330-1332.

[24] J. Lake, *Acta crystallographica*, 1967, **23**, 191-194.

[25] C. Rehm, L. de Campo, A. Brule, F. Darmann, F. Bartsch and A. Berry, *Journal of Applied Crystallography*, 2018, **51**, 1-8.

[26] A. Guinier and G. Fournet, *J. Wiley & Sons, New York*, 1955.

[27] B. Hammouda, *Journal of Applied Crystallography*, 2010, **43**, 716-719.

[28] M. Singh, I. Sinha, A. Singh and R. Mandal, *Colloids and Surfaces A: Physicochemical and Engineering Aspects*, 2011, **384**, 668-674.

[29] S. H. Kim, S. Han, H. Ha, J. Y. Byun and M.-H. Kim, *Catalysis Today*, 2016, **260**, 46-54.

[30] S. L. Pesek, X. Li, B. Hammouda, K. Hong and R. Verduzco, *Macromolecules*, 2013, **46**, 6998-7005.

[31] S. H. Madani, I. H. Arellano, J. P. Mata and P. Pendleton, *Powder Technology*, 2018, **327**, 96-108.

[32] C. C. Ruiz, J. Molina-Bolívar, J. Aguiar, G. MacIsaac, S. Moroze and R. Palepu, *Colloid and Polymer Science*, 2003, **281**, 531-541.

[33] G. Bryant, T. Mortensen, S. Henderson, S. Williams and W. van Megen, *Journal of colloid and interface science*, 1999, **216**, 401-408.

[34] S. Phan, S. Salentinig, E. Gilbert, T. A. Darwish, A. Hawley, R. Nixon-Luke, G. Bryant and B. J. Boyd, *Journal of colloid and interface science*, 2015, **449**, 160-166.

[35] R. K. Mahajan, J. Chawla, K. K. Vohra and V. K. Aswal, *Journal of Applied Polymer Science*, 2010, **117**, 3038-3046.

[36] L. A. Feigin, D. I. Svergun and G. W. Taylor, in *Structure Analysis by Small-Angle X-Ray and Neutron Scattering*, ed. G. W. Taylor, Springer US, Boston, MA, 1987, DOI: 10.1007/978-1-4757-6624-0_2, pp. 25-55.

[37] A. L. R. de Souza, T. Andreani, F. M. Nunes, D. L. Cassimiro, A. E. de Almeida, C. A. Ribeiro, V. H. V. Sarmento, M. P. D. Gremião, A. M. Silva and E. B. Souto, *Journal of Thermal Analysis and Calorimetry*, 2012, **108**, 353-360.

[38] T. Maruyama, M. Nakajima, S. Ichikawa, Y. Sano, H. Nabetani, S. Furusaki and M. Seki, *Bioscience, Biotechnology, and Biochemistry*, 2001, **65**, 1003-1006.

(a)

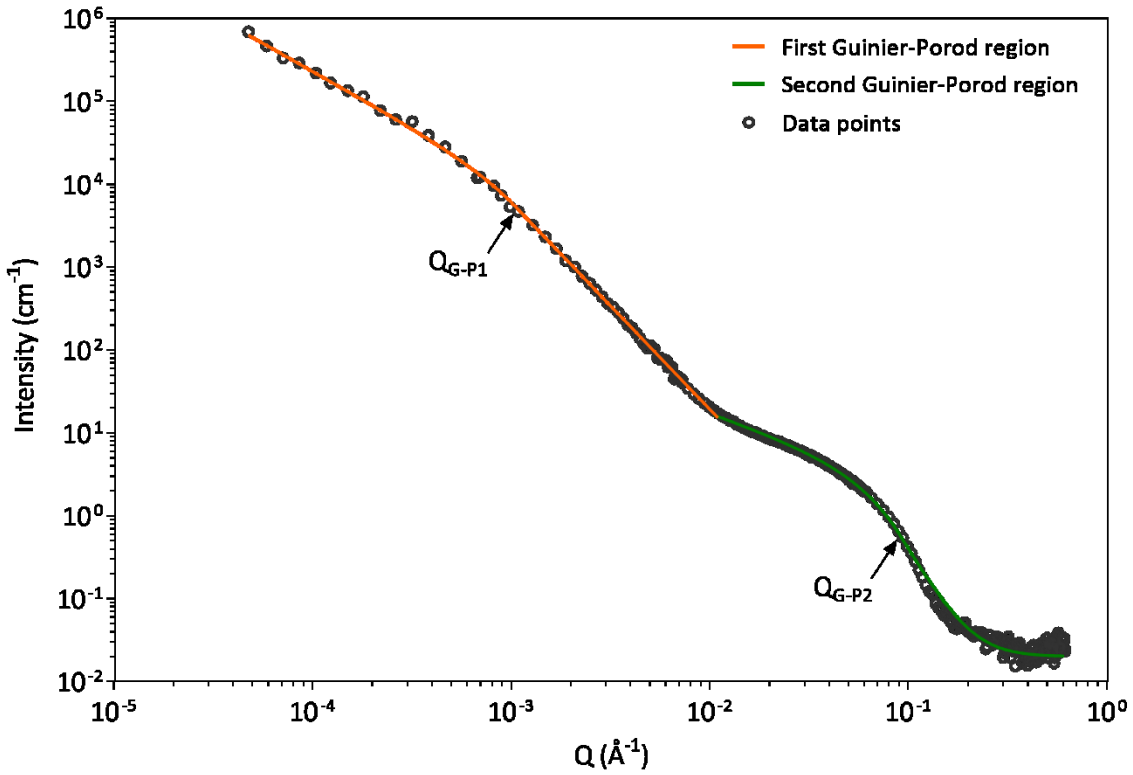

(b)

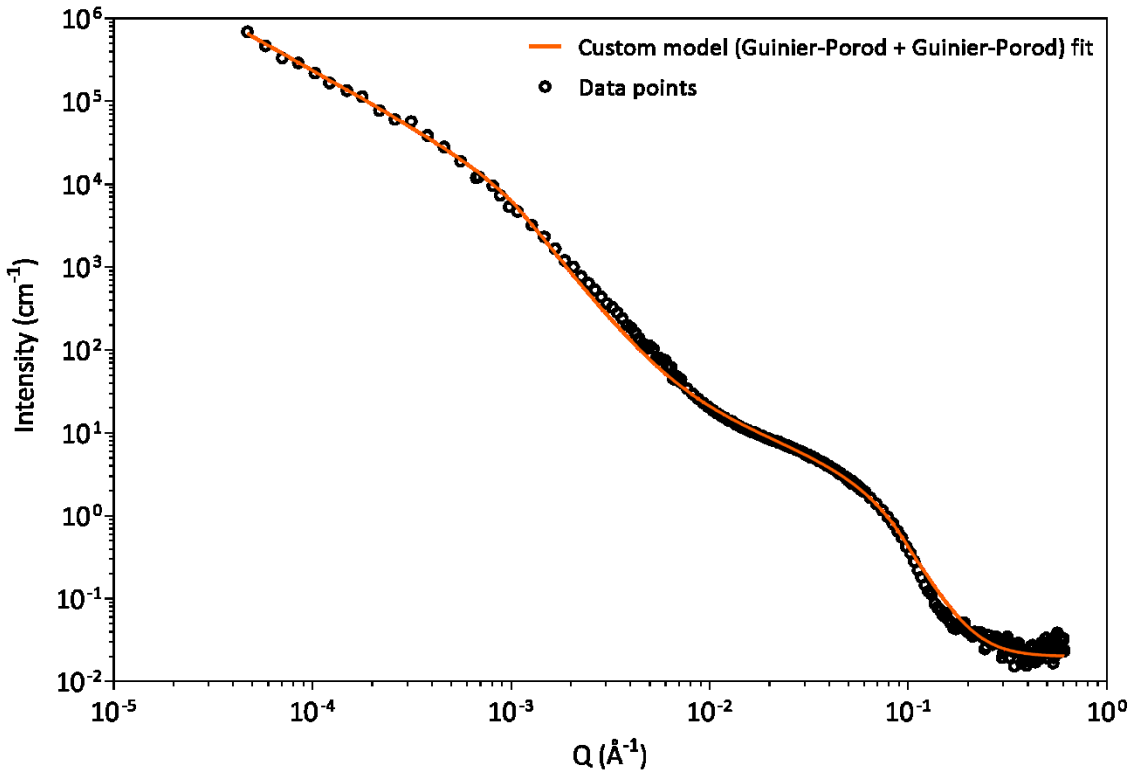

(c)

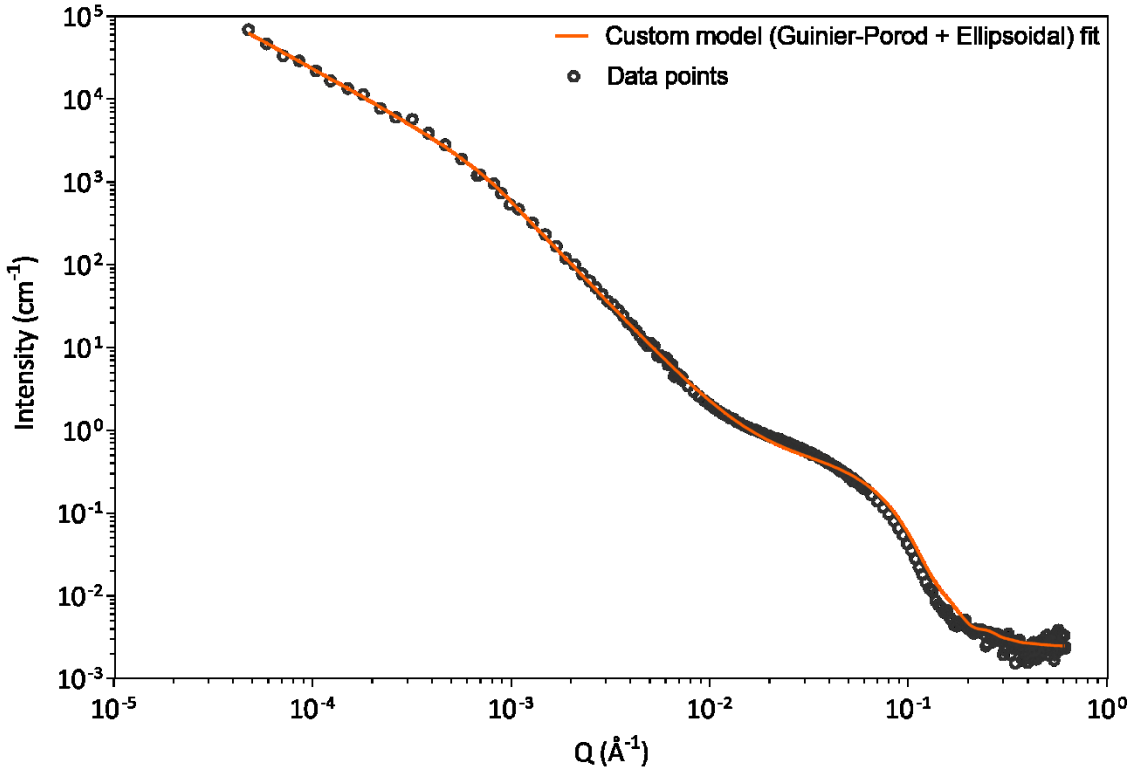


**Figure 1. Model fits to the merged data from SLNs. (a) Generalized Guinier-Porod model fits.** In the figure, ⟝ indicates model within $4.7 \times 10^{-5}$ Å$^{-1}$ ≤ Q ≤ $1.1 \times 10^{-2}$ Å$^{-1}$ and ⟝ indicates model fit within $1 \times 10^{-2}$ Å$^{-1}$ ≤ Q ≤ $6 \times 10^{-1}$ Å$^{-1}$. $Q_{G\text{-}P1} = 9.871 \times 10^{-4}$ Å$^{-1}$ and $Q_{G\text{-}P2} = 9.021 \times 10^{-2}$ Å$^{-1}$. **(b) Customized model (Guinier-Porod + Guinier-Porod) fit.** In the figure, ⟝ indicates model fit within entire Q range i.e. $4.71 \times 10^{-5}$ Å$^{-1}$ ≤ Q ≤ $6 \times 10^{-1}$ Å$^{-1}$. **(c) Customized model (Guinier-Porod + ellipsoidal) fit.** In the figure, ⟝ indicates model fit within entire Q range i.e. $4.71 \times 10^{-5}$ Å$^{-1}$ ≤ Q ≤ $6 \times 10^{-1}$ Å$^{-1}$.

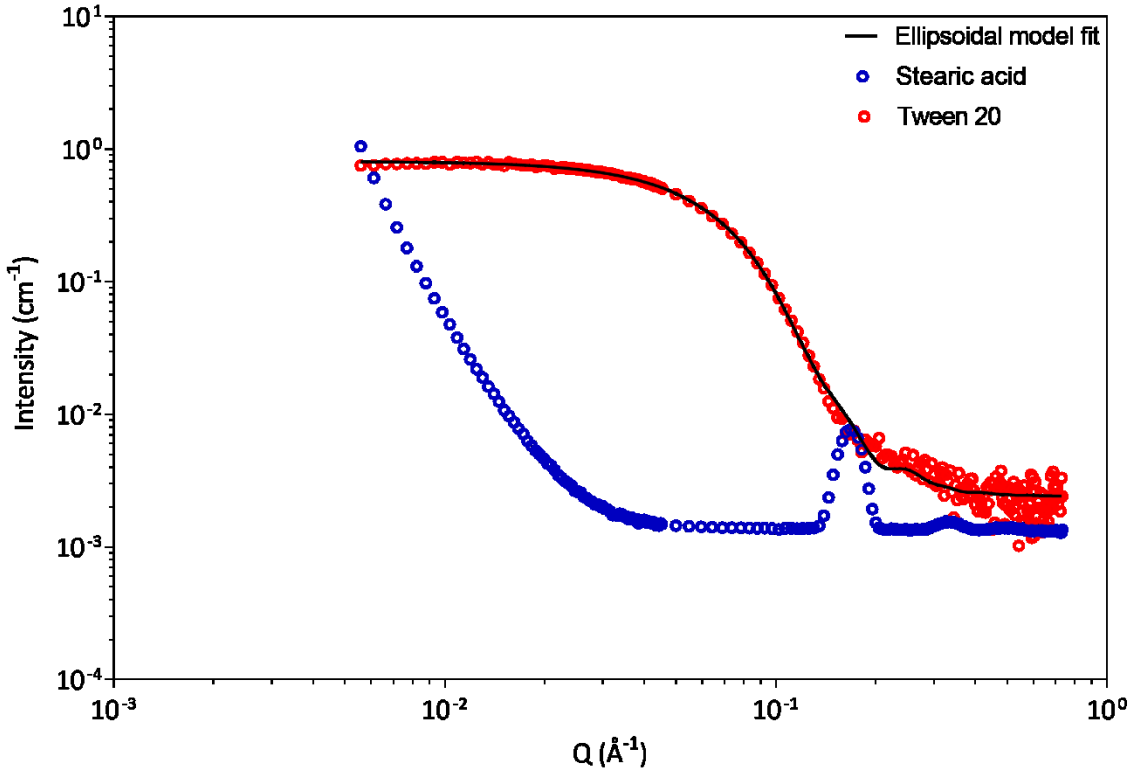


**Figure 2. SANS data from stearic acid and Tween 20 at volume fractions equivalent to that used in SLN preparation.** In the figure, o indicates SANS data from stearic acid crystals suspended in $D_2O$, o indicates SANS data from Tween 20 in $D_2O$ and — indicates ellipsoidal model fit to the SANS data from Tween 20 in $D_2O$.

**Table 1. Porod Exponents and the physical forms they represent.**[27]

| Porod Exponent | Physical form of the scattering entity |
|---|---|
| 4 | • Particles with smooth surfaces |
| 3 | • Particles with very rough surfaces<br>• 'Collapsed' polymer chains (in a bad solvent) |
| 2 | • Two-dimensional structures such as lamellae or platelets<br>• Gaussian polymer chains |
| 5/3 | • 'Fully swollen' polymer chains (in a good solvent) |
| 1 | • Thin cylinder or a rigid rod |

**Table 2. Generalized Guinier-Porod model fit parameters.**

| Parameter | First Guinier-Porod region | Second Guinier-Porod Region |
|---|---|---|
| $Q_{min}$ ($Å^{-1}$) | $4.7 \times 10^{-5}$ | $1 \times 10^{-2}$ |
| $Q_{max}$ ($Å^{-1}$) | $1.1 \times 10^{-2}$ | $6 \times 10^{-1}$ |
| $R_g$ | 1001.3 ± 43.6 Å | 20.3 ± 0.1 Å |
| S | 1.33 ± 0.02 | 0.84 ± 0.01 |
| $D_p$ | 1.67 ± 0.02 | 2.16 ± 0.01 |
| d (fixed) | 2.5 | 4.0 |
| Scale | 0.1098 | 0.0349 |
| Background (fixed) | 0 | 0.0024 |
| $X^2$ | 6.86 | 5.91 |

**The table of contents entry**

**Neutron scattering techniques were successfully used to probe the hierarchical structure of Solid Lipid Nanoparticles (SLNs).** The results indicated multi-length scale structure of SLNs having polydispersed large particles with roughened surfaces at the microscale level and at the nanoscale level, the SLNs solution have an ellipsoidal shape intermediate between spheres and rods, with a crossover from mass fractals to surface fractals.

**Keywords:** small angle neutron scattering (SANS), ultra-small angle neutron scattering (USANS), solid lipid nanoparticles, Guinier-Porod model, ellipsoidal model

R. M. Shah*, J. P. Mata, G. Bryant, L. de Campo, A. Ife, A. V. Karpe, S. R. Jadhav, D. S. Eldridge, E. A. Palombo, I. H. Harding

**Structure Analysis of Solid Lipid Nanoparticles for Drug Delivery: A Combined USANS/SANS Study**

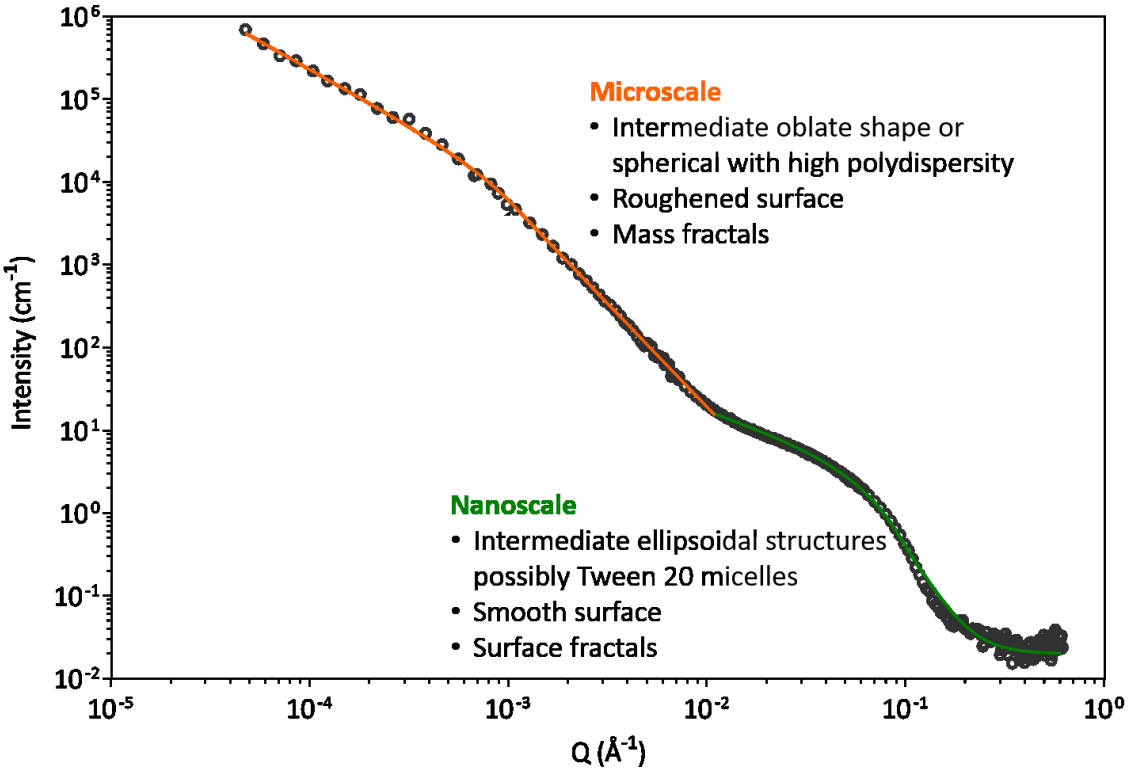

**Author/s:**
Shah, RM; Mata, JP; Bryant, G; de Campo, L; Ife, A; Karpe, AV; Jadhav, SR; Eldridge, DS; Palombo, EA; Harding, IH

**Title:**
Structure Analysis of Solid Lipid Nanoparticles for Drug Delivery: A Combined USANS/SANS Study

**Date:**
2019-01-01

**Citation:**
Shah, R. M., Mata, J. P., Bryant, G., de Campo, L., Ife, A., Karpe, A. V., Jadhav, S. R., Eldridge, D. S., Palombo, E. A. & Harding, I. H. (2019). Structure Analysis of Solid Lipid Nanoparticles for Drug Delivery: A Combined USANS/SANS Study. PARTICLE & PARTICLE SYSTEMS CHARACTERIZATION, 36 (1), https://doi.org/10.1002/ppsc.201800359.